Available online at www.sciencedirect.com

SciVerse ScienceDirect

Solar Energy 86 (2012) 2986–2995

SOLAR ENERGY

www.elsevier.com/locate/solener

Terminal sliding mode control for maximum power point tracking of photovoltaic power generation systems

Chian-Song Chiu*, Ya-Lun Ouyang, Chan-Yu Ku

Department of Electrical Engineering, Chung-Yuan Christian University, Chung-Li 32023, Taiwan

Received 31 March 2011; received in revised form 5 June 2012; accepted 7 July 2012
Available online 2 August 2012

Communicated by: Associate Editor Elias Stefanakos

Abstract

This paper presents a novel terminal sliding mode control (TSMC) method for maximum power tracking of photovoltaic (PV) power systems. First, an incremental conductance method is used for maximum power point (MPP) searching. It provides good efficiency under rapidly changing atmospheric conditions, but the accuracy for finding the MPP is highly related to the MPP tracking control. Therefore, a TSMC-based controller is developed to regulate the system to the searched reference MPP. Different from traditional sliding mode control, the developed TSMC assures finite convergence time for the MPP tracking. Furthermore, a common singularity problem that exists in traditional TSMC is removed in this paper. Even if considering uncertainty in the PV power system, the TSMC guarantees high robustness. Finally, several simulations and experiments show the expected control performance.

Keywords: Terminal sliding mode control (TSMC); PV power system; Maximum power point tracking

1. Introduction

With the increasing global warming and the diminishing conventional fossil-fuel energy sources, renewable energy sources (solar, wind, and fuel cells, etc.) are attracting more attention as alternative energy sources than before. In particular, solar photovoltaic (PV) energy has been widely utilized in many applications (cf. Qi et al., 2009; Nema et al., 2009; Salas et al., 2009) due to its advantages–direct electric power form, easy maintenance, no noise, etc. From the increasing demand of PV power generation systems for both industrial and residential needs, optimizing the power generation and utilization of solar energy becomes an innegligible issue. To extract more PV energy, maximum power point tracking (MPPT) methods are developed, such as perturb and observe method (Salameh and Taylor, 1990; Petreus et al., 2011), incremental conductance method (Hussein et al., 1995), fuzzy logic method (Altasa and Sharaf, 2008; Lalouni et al., 2009; Kottas et al., 2006), and neural network method (Taherbaneh and Faez, 2007). Unfortunately, the maximum power produced by the PV array changes with solar radiation and cell temperature, so that most MPPT methods lack strict convergence analysis and only provide near-maximum power. Although some works (Patcharaprakiti et al., 2005; Solodovnik et al., 2004) propose nonlinear MPPT control with guaranteed stability, these approaches are difficultly realized due to assuming exactly known power converter model and using the time derivative of the PV voltage and current.

To obtain easy implementation and assured stability, maximum power voltage (MPV) based approaches (Hua

* Corresponding author. Address: Department of Electrical Engineering, Chung-Yuan Christian University, 200, Chung Pei Rd., Chung-Li 32023, Taiwan. Tel.: +886 3 265 4816; fax: +886 3 265 4899.
E-mail addresses: acs.chiu@gmail.com (C.-S. Chiu), g9478025@cycu.edu.tw (Y.-L. Ouyang), cku5@ford.com (C.-Y. Ku).

0038-092X/$ - see front matter © 2012 Elsevier Ltd. All rights reserved.
http://dx.doi.org/10.1016/j.solener.2012.07.008

Nomenclature

ΔV	update parameter for MPP searching
λ	solar insolation (mW/cm^2)
A	ideal P–N junction characteristic factor
C_1	input capacitance of the boost converter (F)
C_2	output capacitance (F)
d	duty ratio of the PWM control input signal
E_{go}	semiconductor band-gap energy (1.1 ev)
i_L	current on the inductance L (A)
i_{or}	PV array reverse saturation current (A)
i_{ph}	PV array light-generated current (A)
i_{pv}	PV array output DC current (A)
i_{rs}	PV array reverse saturation current at the reference temperature (A)
i_{scr}	short-circuit cell current at the reference temperature and insolation (A)
K_l	PV array short-circuit current temperature coefficient (A/K)
K_o	Boltzmann's constant (1.3805×10^{-23} J/K)
L	inductor inductance of the boost converter (H)
N_p	number of parallel cell of the PV array
N_s	number of series cell of the PV array
q	electrical charge (1.6×10^{-19} C)
R	load resistance (Ω)
R_C	internal resistance on the capacitance C_2 (Ω)
T	PV array cell temperature (K)
T_r	PV array reference temperature (K)
V_D	forward voltage of the power diode (V)
V_{C2}	voltage over the capacitor C_2 (V)
V_{pvd}	reference maximum power PV voltage (V)
V_{pv}	PV array output DC voltage (V)

et al., 1998; Kim, 2007; Koutroulis et al., 2001; Veerachary et al., 2003) are developed using a two-loop MPPT control scheme. In detail, the first loop is to determine the MPV reference of the PV array, and the second loop is to regulate the PV array voltage to the reference voltage. The procedure repeats the MPV reference searching and the PV voltage tracking until the maximum power is reached. The advantage is that some traditional MPPT algorithms, for example, incremental conductance method, perturb and observe method, etc., can be realized with guaranteed convergence stability. However, the tracking performance is highly dependent to the performance of the tracking controller in the second loop. The existing disturbances and uncertainties will also affect the control results. We can see that most of MPV based approaches renders to power chattering around the MPP (Hua et al., 1998; Kim, 2007; Koutroulis et al., 2001). In other words, the MPV based MPPT needs to be improved.

Sliding mode control (Slotine and Li, 1991) has powerful ability for the control of uncertain systems; therefore, the controlled system with sliding mode exhibits robustness properties with respect to both internal parameter uncertainties and external disturbances. Although the convergence rate of SMC may be arbitrarily fast via appropriate parameters, it provides only asymptotically stable and infinite time convergence. From the pioneering work of Venkataraman and Gulati, 1993, terminal sliding mode control (TSMC) achieves finite-time convergence stability. With this ability, the closed loop system can be accurately and efficiently controlled to the given command. Accordingly, many application examples of TSMC have been considered to provide fast and finite time control performance as well as high precision (Chang et al., 2008; Feng et al., 2002; Huang et al., 2005; Min and Xu, 2009). In light of this, if the TMSC can be applied to the PV voltage tracking, the MPV based MPPT will provide better control performance. However, due to the use of fractional power functions as the sliding hyperplane, there exist intrinsic singular problems (Chang et al., 2008; Tao et al., 2004; Parra-Vega and Hirzinger, 2004; Barambones and Etxebarria, 2002; Man and Yu, 1997). Therefore, all of the above motivate us to improve the TSMC method for the MPPT of PV power systems.

In this paper, a TSMC-based MPPT scheme for stand-alone PV power generation systems is developed via the MPV based design. In the first loop, the MPV reference is obtained from the incremental conductance method. By taking a DC/DC boost converter as the power control circuit, novel TMSC is proposed to drive the system to the MPV reference in the second loop. Moreover, the aforementioned singularity problem is removed by proposing a new terminal sliding surface. With the advantage of finite-time convergence in TMSC, the MPP is accurately followed such that the generated PV power is increased. Meanwhile, the robustness against disturbance and system parameter uncertainties of the DC/DC boost converter is guaranteed. Compared with the traditional MPV based MPPT of PV systems, the proposed method provides finite time PV voltage tracking so that fewer power oscillation is induced by MPP searching (i.e., more stable power generation is obtained).

The rest of the paper is organized as follows. The electric characteristic of PV array system is presented in Section 2. MPP searching via incremental conductance and power tracking via TSMC are addressed in Sections 3.1 and 3.2, respectively. Next, the robustness issue for the proposed TMSC is presented in Section 3.3. Numerical simulations and experiments for both fixed and varying atmosphere are given in Sections 4 and 5. Finally, some conclusions are made in Section 6.

2. Electrical characteristics of photovoltaic power generation system

Referring Salas et al. (2009) and Kim (2007), the electric characteristic of the PV array can be described by the current equation:

$$i_{pv} = N_p i_{ph} - N_p i_{rs}(e^{qV_{pv}/N_s A K_o T} - 1)$$

where V_{pv} and i_{pv} denote the output voltage and current of the PV array, respectively; N_p and N_s are the number of the parallel and series cells, respectively; T is the cell temperature; the electronic charge $q = 1.6 \times 10^{-19}$ C; Boltzmann's constant $K_o = 1.3805 \times 10^{-23}$ J/K; the ideal P–N junction characteristic factor $A = 1$–5; i_{ph} is the light-generated current; i_{rs} denotes the reverse saturation current; and the intrinsic shunt and series resistances are neglected. Besides, i_{rs} and i_{ph} are functional of solar insolation and cell temperature in the following form:

$$i_{rs} = i_{or}(T/T_r)^3 e^{qE_{go}/(1/T_r - 1/T)/AK_o}$$
$$i_{ph} = ((i_{scr} + K_l(T - T_r))\lambda/100$$

where i_{or} is the reverse saturation current at the reference temperature T_r; i_{scr} is the short-circuit cell current at reference temperature and reference insolation 100 mW/cm^2; $E_{go} = 1.1$ eV is the band-gap energy of the semiconductor making up the cell; K_l (A/K) is the short-circuit current temperature coefficient; and λ is the insolation in $mW/$cm^2. It is straightforward to obtain the PV power:

$$P_{pv} = i_{pv} V_{pv} = N_p i_{pv} V_{pv} - N_p i_{rs} V_{pv}(e^{qV_{pv}/N_s A K_o T} - 1) \tag{1}$$

To show the electric feature, we depict the power-voltage characteristic diagram of a PV array as shown in Fig. 1. Obviously, the maximum power changes along various insolation and cell temperature. Furthermore, there exists a unique V_{pv} such that the output PV power is maximized.

To adjust the PV array output voltage V_{pv} for maximizing the solar power generation, a DC/DC boost converter is connected as the configuration shown in Fig. 2. The boost converter carries out the power conversion on the PV array terminal, indirectly controlling the operation point of the PV array and its power generation. In other words, the PV array can be viewed with an active power load whose value can be adjusted through the duty cycle of the converter. On the other hand, by using the time average method (Krein et al., 1992; Sun and Gratstollen, 1992), the dynamics of the boost converter with the PV array is written as:

$$\begin{aligned}
\dot{V}_{pv} &= \frac{-1}{C_1} i_L + \frac{i_{pv}}{C_1} \\
\dot{i}_L &= \frac{1}{L} V_{pv} - \frac{R_C(1-d)}{L\left(1+\frac{R_C}{R}\right)} i_L + \frac{1-d}{L}\left(\frac{R_C}{R+R_C} - 1\right) V_{C2} \\
&\quad - \frac{V_D(1-d)}{L} \\
\dot{V}_{C2} &= \frac{1-d}{C_2\left(1+\frac{R_C}{R}\right)} i_L - \frac{1}{C_2(R+R_C)} V_{C2}
\end{aligned} \tag{2}$$

where V_{pv}, V_{C2}, and i_L are the PV array voltage (i.e., the voltage of the capacitance C_1), the voltage of the capacitance C_2, and the current on the inductance L, respectively; R_C is the internal resistance on the capacitance C_2; V_D is the forward voltage of the power diode; d is the duty ratio of the PWM control input signal; R is the load resistance. From above, since the PV array power is maximized by a specific PV array voltage V_{pv} under a fixed insolation and temperature. The control objective is to design the PWM control input d such that $V_{pv}(t)$ is moved to the MPP. To achieve the objective, a terminal sliding mode controller is proposed in the following.

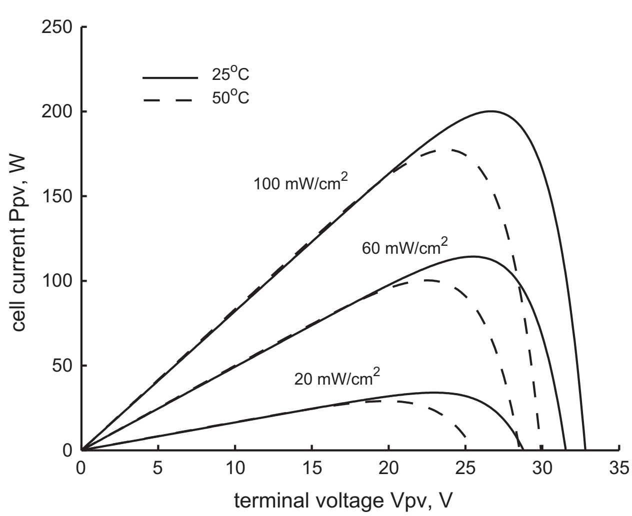

Fig. 1. Power distribution of a 200 W PV array panel.

3. Terminal sliding mode MPPT controller

To achieve MPP under the changing atmosphere, the overall control structure is illustrated in Fig. 3. Here, i_{pv} and V_{pv} are measured from PV array and sent to the MPP searching algorithm, which generates the reference maximum power voltage V_{pvd}. Then, the reference voltage V_{pvd} is given to the MPV-based TSMC controller for the maximum power tracking.

3.1. MPP searching algorithm

To achieve the maximum power operation, we use an incremental conductance method (cf. Salas et al., 2009; Hussein et al., 1995) to search the MPP voltage V_{pvd}. According to the electric power Eq. (1), the power slope dP_{pv}/dV_{pv} can be expressed as

$$\frac{dP_{pv}}{dV_{pv}} = i_{pv} + V_{pv}\frac{di_{pv}}{dV_{pv}} \tag{3}$$

When the power slope $dP_{pv}/dV_{pv} = 0$, i.e., $\frac{di_{pv}}{dV_{pv}} = -\frac{i_{pv}}{V_{pv}}$, the PV system operates at the maximum power generation. Therefore, the update law for V_{pvd} is given by the following rules:

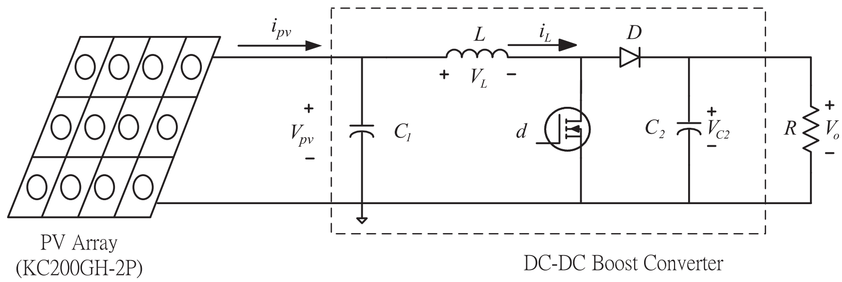

Fig. 2. Solar power generating system with a 200 W PV array and a DC–DC boost converter.

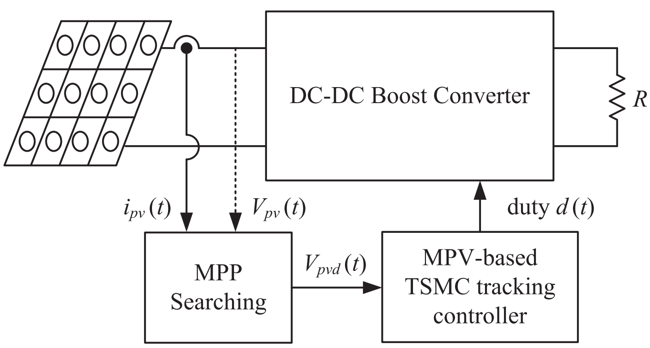

Fig. 3. MPPT structure using the two-loop algorithm.

$$\begin{cases} V_{pvd}(k) = V_{pvd}(k-1) + \Delta V, & \text{for } \frac{di_{pv}}{dV_{pv}} > -\frac{i_{pv}}{V_{pv}} \\ V_{pvd}(k) = V_{pvd}(k-1) - \Delta V, & \text{for } \frac{di_{pv}}{dV_{pv}} < -\frac{i_{pv}}{V_{pv}} \end{cases} \tag{4}$$

where $V_{pvd}(k)$ is the reference MPV at kth step; ΔV is the update parameter which can be adjusted based on the experiment settings. The flowchart of the searching procedure can be concluded as Fig. 4. After iterative adjusting the value of V_{pvd}, the maximum power condition is achieved by $\frac{dP_{pv}}{dV_{pv}} \simeq 0$. Thus, the problem is changed to control the PV array voltage V_{pv} to follow the reference MPV V_{pvd}.

Remark 1. For the V_{pvd} updating law (4), the PV voltage tracking result will affect the MPP searching in the next step. Since the MPP searching is highly dependent to the MPV tracking controller, there exist the following problems: (1) Power wastage occurs once the controller response is too slow; and (2) Miscalculation of the V_{pvd} arises if the controller results in oscillation. Therefore, an appropriate MPV tracking controller is required not only to guarantee the convergence with the given reference, but also to enhance the MPP searching performance. The best is V_{pv} always follow the reference MPP voltage V_{pvd}.

Remark 2. If the controller in the second loop is well designed with assured fast tracking performance, larger update parameter ΔV usually results in better transient response. However, there might exist chattering at the steady state if ΔV is too large. Thus, the update parameter ΔV requires trade-off tuning.

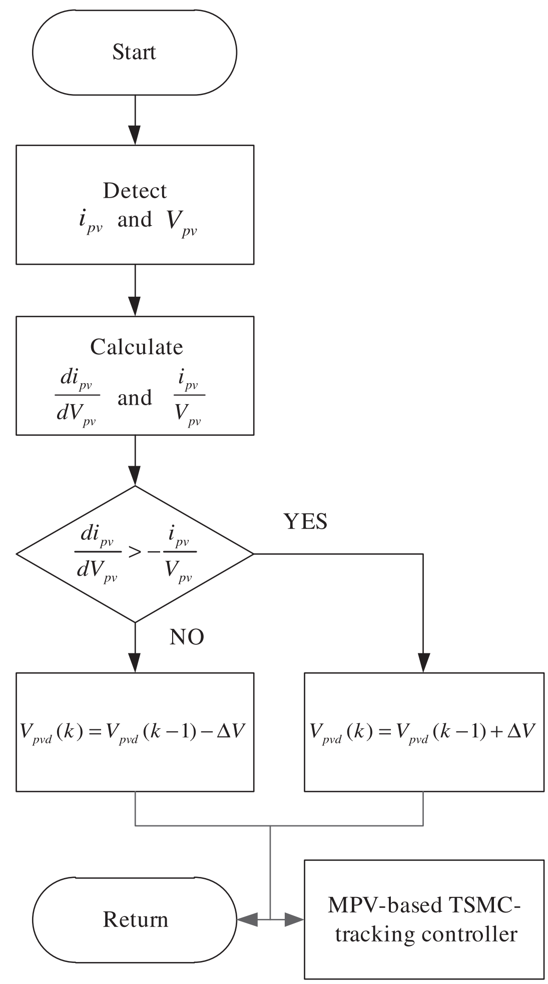

Fig. 4. Flow chart of the maximum power voltage searching algorithm.

3.2. Terminal sliding mode controller

Before the controller design, let $x_1(t) = V_{pv}(t)$, $x_2(t) = i_L(t)$, $x_3(t) = V_{C2}(t)$, $x_{1d}(t) = V_{pvd}(t)$ and the system dynamics (2) is rewritten as follows:

$$\begin{aligned} \dot{x}_1 &= \frac{1}{C_1}\left(-x_2 + i_{pv}\right) \\ \dot{x}_2 &= f_1(x) + g_1(x)d(t) \\ \dot{x}_3 &= f_2(x) + g_2(x)d(t) \end{aligned} \tag{5}$$

where $x = [x_1\ x_2\ x_3]^T$;

$$f_1(x) = \frac{x_1}{L} - \frac{R_C}{L\left(1+\frac{R_C}{R}\right)}x_2 + \frac{1}{L}\left(\frac{R_C}{R+R_C} - 1\right)x_3 - \frac{V_D}{L} \tag{6}$$

$$g_1(x) = -\frac{R_C}{L\left(1+\frac{R_C}{R}\right)}x_2 - \frac{1}{L}\left(\frac{R_C}{R+R_C} - 1\right)x_3 + \frac{V_D}{L} \tag{7}$$

$$f_2(x) = \frac{1}{C_2\left(1+\frac{R_C}{R}\right)}x_2 - \frac{1}{C_2(R+R_C)}x_3 \tag{8}$$

$$g_2(x) = -\frac{1}{C_2\left(1+\frac{R_C}{R}\right)}x_2. \tag{9}$$

To achieve the maximum power tracking, the terminal sliding mode controller is proposed to let PV voltage V_{pv} track the reference MPV V_{pvd}. Once V_{pv} always follows V_{pvd}, the PV power system will move to the maximum power point along the incremental conductance adjusting. First, let us define the voltage tracking error and take its time derivative below:

$$\begin{aligned} e_1 &= x_1 - x_{1d} \\ \dot{e}_1 &= \frac{1}{C_1}(-x_2 + i_{pv}) - \dot{x}_{1d}. \end{aligned} \tag{10}$$

By taking x_2 as a virtual control input, we define an auxiliary tracking error $e_2 = x_2 - x_{2d}$ with $x_{2d} = i_{pv} - C_1\dot{x}_{1d}$. Then the new dynamics is obtained as follows:

$$\dot{e}_1 = \frac{-e_2}{C_1} \tag{11}$$

$$\dot{e}_2 = f_1(x) - \dot{x}_{2d} + g_1(x)d(t) \tag{12}$$

where $\dot{x}_{2d} = \dot{i}_{pv} - C_1\ddot{x}_{1d}$. The control problem becomes designing the control law $d(t)$ to achieve the fast convergence of e_1 and e_2. To this end, a terminal sliding mode function $s(t)$ is defined as

$$s = e_2^r - \alpha e_1 \tag{13}$$

where $\alpha > 0$, $r = p/q$, with $1 < r < 2$; p and q are odd integers satisfying $0 < q < p < 2q$. If $s(t)$ is always kept at zero such that

$$e_2 = \alpha^{1/r} e_1^{1/r}, \tag{14}$$

the error Eq. (11) becomes

$$\dot{e}_1 = -\frac{\alpha^{1/r}}{C_1} e_1^{1/r} \tag{15}$$

by substituting (14) into (11). Obviously, from solving the error dynamic Eq. (15), e_1 converges to zero in finite time:

$$t_{e1} = C_1 \frac{|e_1(0)|^{1-\frac{q}{p}}}{\alpha^{q/p}\left(1-\frac{q}{p}\right)} \tag{16}$$

Due to the fact $e_2 = \alpha^{1/r} e_1^{1/r}$ on the surface $s(t) = 0$, the convergence of the tracking error e_2 is accomplished in the same finite time (16). As a result, if the system is driven to the sliding surface $s(t) = 0$, the errors e_1 and e_2 will converge to zero in finite time, i.e., V_{pv} always follows the MPP voltage V_{pvd}.

Next, based on the definition of the sliding mode function, the time derivative of the terminal sliding function $s(t)$ along (11) and (12) simply arrives with

$$\begin{aligned} \dot{s} &= re_2^{r-1}\dot{e}_2 - \alpha\dot{e}_1 \\ &= re_2^{r-1}[f_1(x) - \dot{x}_{2d}(t) + g_1(x)d(t)] + \frac{\alpha e_2}{C_1} \end{aligned} \tag{17}$$

For driving $s(t)$ to zero, the control input $d(t)$ is designed as follows:

$$d(t) = \frac{1}{g_1(x)}\left[\frac{-\alpha e_2^{2-r}}{rC_1} - f_1(x) + \dot{x}_{2d}(t) - K\mathrm{sign}(s)\right] \tag{18}$$

where $K > 0$ and $g_1(x) \neq 0$ for all $x(t)$. By substituting the above control law into the dynamics (17), the closed-loop system is obtained below:

$$\dot{s} = -K \cdot re_2^{r-1}\mathrm{sign}(s) \tag{19}$$

Afterward, the TSMC design achieves MPV tracking with the following theorem where the detailed stability condition can be proved as given in Appendix A.

Theorem 1. *Consider the PV array power generation system (2) using the TMSC controller (18) with $K > 0$. The closed-loop control system is ensured with finite-time convergence for the MPP voltage tracking.*

Remark 3. In traditional sliding mode control, the convergence time for the system states is infinite, i.e., in the form of asymptotical convergence. In comparison, TSMC is used in this paper for more accurate tracking control, and with the ability of finite time convergence. Moreover, traditional TMSC sets $s(t) = e_2 - \alpha e_1^{1/r}$ such that $\dot{s}(t)$ will lead to singularity on the error terms. On the contrary, the proposed TSMC using the terminal sliding function (13) does not have the singularity problem.

3.3. Robustness analysis

For more general PV maximum power tracking purpose, the boost converter system is considered as an uncertain form due to the existence of the uncertainties from the passive components. To this end, a controller gain redesign is developed to enhance the robustness of the controlled system.

Assume the system with uncertainties in the form:

$$\begin{aligned} f_1 &= \hat{f}_1 + \Delta f_1 \\ g_1 &= \hat{g}_1 + \Delta g_1 \\ \dot{x}_{2d} &= \hat{h}_c + \Delta h_c \end{aligned} \tag{20}$$

where $\hat{f}_1$, $\hat{g}_1$, and $\hat{h}_c$ are known and measurable; Δf_1, Δg_1, and Δh_c are the uncertain parts arising from system uncertainties and measurement errors (e.g. calculation error of i_{pv}). Meanwhile, the uncertainties satisfy the following boundary conditions

$$\varpi^{-1} \leqslant \hat{g}_1/g_1 \leqslant \varpi \tag{21}$$

$$|\Delta f_1| < F \tag{22}$$

$$|\Delta h_c| < H \tag{23}$$

where $\hat{g}_1,\ g_1 \neq 0$ and $0 < \varpi < 1$; F and H are known upper bounds of the uncertain dynamics of Δf_1 and Δh_c, respectively. It is worthwhile to note that $\hat{h}_c$ is the nominal part of $\dot{x}_{2d}$, which is obtained from the difference approximation of $\dot{x}_{2d}$. In other words, the term Δh_c presents the derivative approximation error. Furthermore, the measurement errors and current ripples on i_{pv} and i_L can be included in the uncertainties Δf_1, Δg_1, and Δh_c. This means that the robustness satisfies generality. From the terminal sliding function (13), its derivative with uncertainties is written as

$$\dot{s} = re_2^{r-1}[\hat{f}_1 + \Delta f_1 - \hat{h}_c - \Delta h_c + (\hat{g}_1 + \Delta g_1)d(t)] + \frac{\alpha e_2}{C_1} \tag{24}$$

and the control law is modified as follows

$$d(t) = \frac{1}{\hat{g}_1}\left[\frac{-\alpha e_2^{2-r}}{rC_1} - \hat{f}_1 + \hat{h}_c - K^* \mathrm{sign}(s)\right] \tag{25}$$

Submitting (25) into (24) results in the following equation:

$$\dot{s} = re_2^{r-1}\left[\Delta f_1 - \Delta h_c - g_1\hat{g}_1^{-1}K^*\mathrm{sign}(s)\right] + re_2^{r-1}(g_1 - \hat{g}_1)\hat{g}_1^{-1}\left(\frac{-\alpha e_2^{2-r}}{rC_1} - \hat{f}_1 + \hat{h}_c\right) \tag{26}$$

Then, the designed TSMC achieves MPP voltage tracking with robustness according to the following theorem where the corresponded proof is presented in Appendix B.

Theorem 2. *Consider the uncertain PV power generation system (2) using the terminal sliding mode control law (25). If the control gain K^* satisfies the following inequality*

$$K^* > \varpi(|\Delta f_1| + |\Delta h_c| + \eta + |\varpi - 1|\left(\frac{\alpha}{rC_1}\left|e_2^{2-r}\right| + |\hat{f}_1| + |\hat{h}_c|\right), \tag{27}$$

then the controlled system achieves a robust MPPT. Furthermore, the finite time convergence of the MPP voltage tracking is guaranteed.

Remark 4. Since the gain condition is held in a locally region, there exists a upper bound for the right hand sided terms of (27). In the implementation, the control gains K^* is a constant chosen by trial and error according to the control response. Larger K^* yields higher robustness.

4. Numerical simulations

For the verification of the MPP control scheme, a PV power generation system is established with a boost converter and a 200 W PV module KC200GH-2P, in which its specification is stated in Table 1. The parameters of the boost converter are chosen as $L = 1.21$ mH, $R_L = 0.15\ \Omega$, $R_C = 39.6\ \Omega$, $C_1 = 1000\ \mu$F, $C_2 = 1000\ \mu$F, $R = 25\ \Omega$, and $V_D = 0.82$ V, where all system parameters are assumed with a 10% deviation. The switching frequency of the converter is set to 50 kHz. To perform the TSMC based MPPT control, the incremental conductance method stated in Section 3.1 is used to determine the reference maximum power voltage V_{pvd}, where the incremental value for each step is $\triangle V = 0.0005$. The frequency of the searching algorithm is set as 10 kHz in this paper to achieve fast MPP searching. On the other hand, the controller parameters are set to $K^* = 300$, $\alpha = 20$, $p = 19$, and $q = 17$. In the following, two scenarios including fixed insolation and varying insolation are simulated to verify the proposed scheme.

Table 1
Specifications of the PV array panel KC200GH-2P.

Parameter	Value
Maximum output power P_{max}	200 W ± 10%
Maximum current i_{max}	7.61 A
Open circuit voltage V_{oc}	32.9 V
Short circuit current i_{scr}	8.21 A
Short circuit current temperature coefficient K_I	4.79×10^{-3} A/°C
P–N junction characteristic factor A	1.8

First, consider a fixed insolation at 100 mW/cm^2 and 25 °C cell temperature. By using the robust TSMC MPPT controller (25), simulation results are obtained as shown from Figs. 5–7. From the result in Fig. 5, the PV power generation system reaches the desired voltage $V_{pvd} = 26.3$ V and maximum power 200 W at 0.1 s. This means that the proposed controller achieves maximum power tracking in finite time and provides high robustness to parameter uncertainties. Furthermore, the control input does not have chattering behavior as in traditional SMC due to the finite time convergence of tracking errors.

Next, consider a varying atmosphere at 25 °C and a sinusoidal varying insolation $60 + 40\sin(0.6\pi t)$.

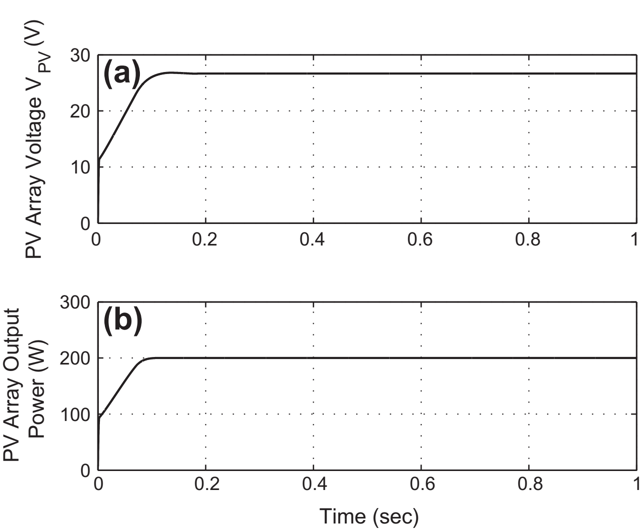

Fig. 5. MPPT control of the PV array (a) voltage V_{pv} and (b) output power P_{pv}.

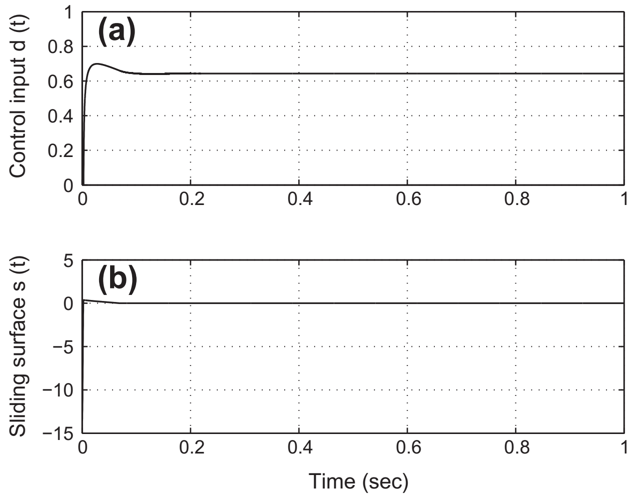

Fig. 6. MPPT control response of the (a) control input $d(t)$ and (b) sliding surface $s(t)$.

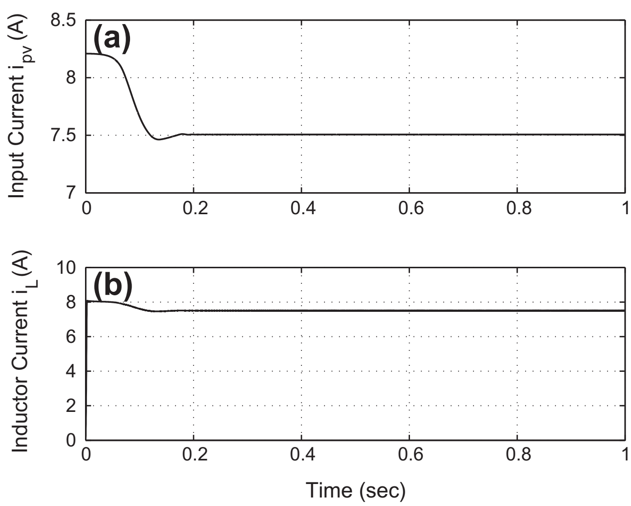

Fig. 7. MPPT control response of the (a) PV array current $i_{pv}(t)$ and (b) inductor current $i_L(t)$.

Meanwhile, a PI controller (Koutroulis et al., 2001) is also applied to compare with designed TSMC. Here the PI controller is set as

$$d(t) = K_p e_1(t) + K_i \int_0^t e_1(\tau) d\tau \tag{28}$$

where the control gains $K_p = 10$ and $K_i = 0.1$ for well reference tracking. With the above settings, the PV MPPT control is performed and renders to the control results for P–V curves given in Fig. 8. As a result, PI controller leads to a larger chattering due to the varying atmosphere and non-exact MPP voltage tracking. In contrast, the MPPT via TMSC results in a smoother response. This implies that the usable output power from the PV array panel is not wasted.

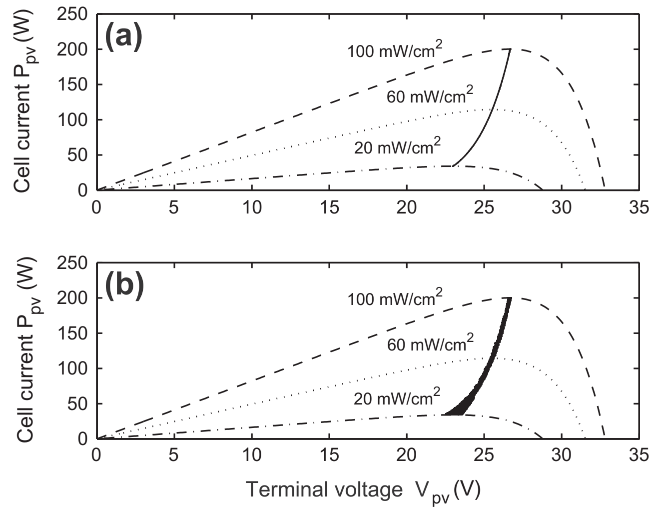

Fig. 8. $P_{pv} - V_{pv}$ curve response under varying insolation using (a) TSMC and (b) PI control at 25 °C.

5. Experiment results

To further verify the validity of the proposed scheme in real-world environment, several experiments of TSMC-based MPPT control are performed in this section. Based on the same system parameter settings as the numerical simulation, the developed TSMC is realized by a DSP-based control card (dSPACE DS1104). The PV voltage, PV current, inductance current, and output voltage of the boost converter are measured through A/D modules and sent to the DS1104 DSP controller board. After the controller is established by using build-up blocks in Matlab–Simulink, real time workshop (RTW) automatically converts *C* code from Simulink and is downloaded to DS1104 controller board. Finally, the control effort is calculated from feedback and then a PWM signal in 50 kHz is directly generated to control the switching MOSFET of the DC/DC boost converter.

Here the control experiments are carried out using three different scenarios: (1) low insolation, (2) high insolation, and (3) whole day observation. Throughout the experiments, the PI controller (Koutroulis et al., 2001) is also utilized to compare the results with TMSC. The comparisons are made under the same conditions where the MPP searching uses the incremental voltage for each computing step is $\triangle V = 0.3$. Moreover, the control gains are set as $K_p = 8$, $K_i = 10$ for the PI controller and $K^* = 2$, $\alpha = 0.03$, $p = 17$, $q = 15$ for TMSC.

5.1. Experiment 1 – Low insolation test

The PV maximum power tracking for low insolation experiment is done under the fixed atmosphere at 22 °C and 35 mW/cm^2 insolation. Furthermore, the controllers activate at 2 s in order to observe the transient response. The PV array output voltage V_{pv} response is shown in Fig. 9, while the power generated from the PV array module is illustrated in Fig. 10. It is clear that the TMSC

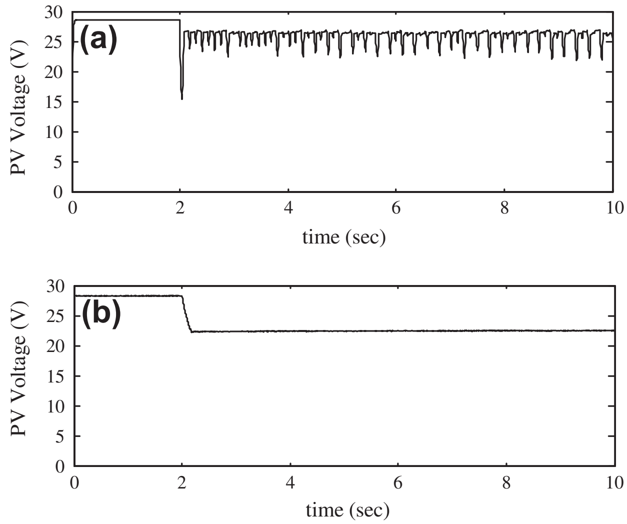

Fig. 9. PV array voltage of (a) PI controller and (b) TSMC at 22 °C and 35 mW/cm^2.

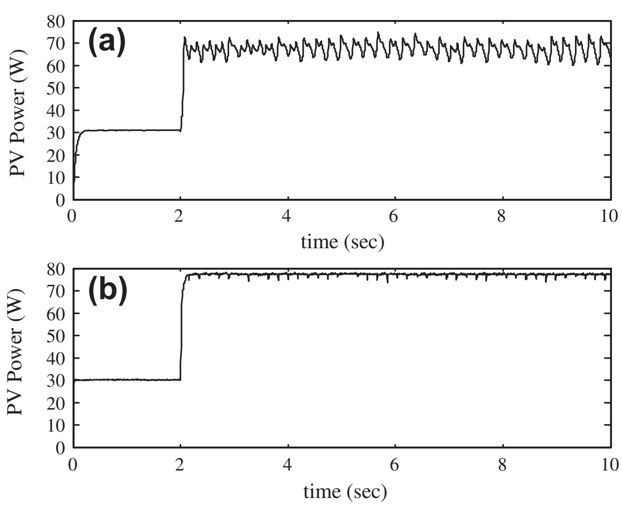

Fig. 10. PV array power of (a) PI controller and (b) TSMC at 22 °C and 35 mW/cm^2.

quickly drives the system to the maximum value 77 W, where the PI controller converges at a much lower power 72 W. From the results, the proposed TMSC has smaller chattering phenomenon and higher power output compared with the PI controller.

5.2. Experiment 2 – High insolation test

Next, the PV maximum power tracking for high insolation is performed under 75 mW/cm^2 at 45 °C. With the same start-up time at $t = 2$ s, the performances including V_{pv} and P_{pv} are given in Figs. 11 and 12, respectively. From the results, the PI controller only drives the PV power system to 120 W, and it accompanies with sufficiently large ripples under high insolation. In contrast, the TMSC generates up to 148 W with much stable output power curve even under high insolation.

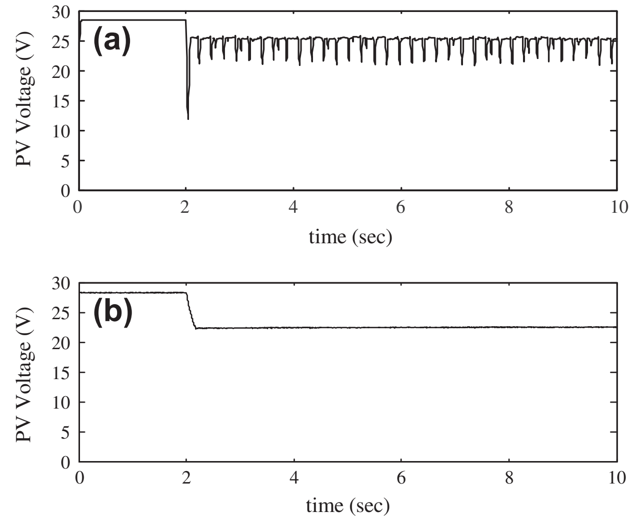

Fig. 11. PV array voltage of (a) PI controller and (b) TSMC at 42 °C and 75 mW/cm^2.

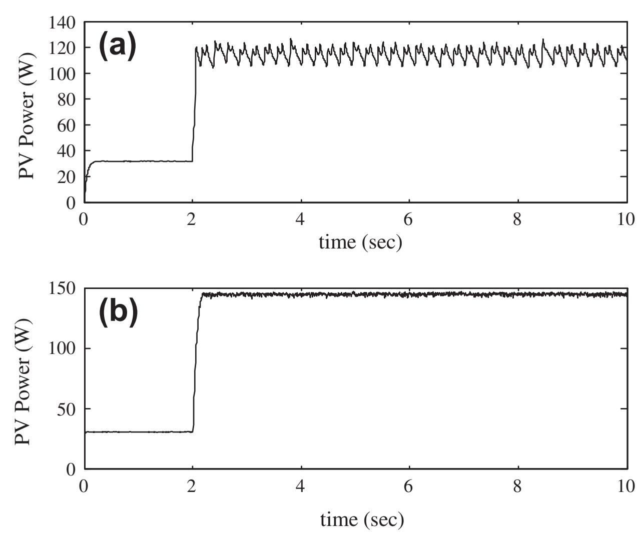

Fig. 12. PV array power of (a) PI controller and (b) TSMC at 42 °C and 75 mW/cm^2.

5.3. Experiment 3 – Whole day test

In this experiment, we measure the control results from 07:00–16:00 to observe the daily generated power where the atmosphere conditions are 20–45 °C and 20–80 mW/cm^2, respectively. Additional open-loop system is compared with the controlled system using the PI controller and robust TSMC. The result is given in Fig. 13 which indicates that TSMC generates more power than the PI controller up to 10% higher. This is reasonable that the chattering response decreases the extracted power in the PI control. Moreover, since the MPP searching is based on the incremental conductance method, the searching result is highly dependent to efficiency of the controller. The faster the controller regulates V_{pv} to V_{pvd}, the better MPP searching

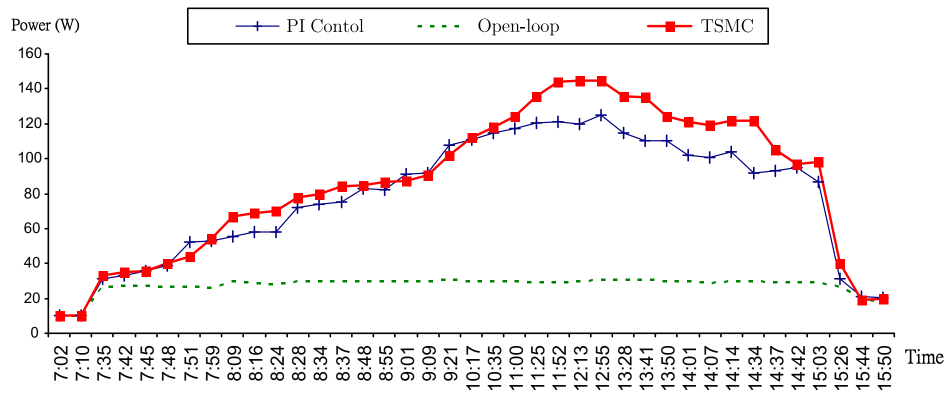

Fig. 13. The comparison result for extracted power using different controllers on the date 2010.11.01 from 07:00 to 16:00.

result is achieved. Therefore, the TSMC provides the ability of fast convergence time and high robustness to the system uncertainties.

Remark 5. Although the well-tuned PI controller will yield zero steady state error and fast tracking response for a slow time-varying tracking reference, the tracking performance is degraded for a rapidly changing tracking reference. Unfortunately, the MPP searching is usually set with fast updating frequency to cope with rapidly changing atmosphere. In contrast, the TSMC has high ability to match the fast MPP searching.

6. Conclusions

In this paper, the robust terminal sliding mode control has been introduced for the maximum power tracking of PV power generation systems. Even considering uncertainties, the controlled system assures finite time convergence of MPP voltage tracking. Moreover, the singular problem of the control law is avoided in comparison with traditional TSMC. By combining the finite-time tracking controller and the incremental conductance method, the MPPT for PV systems is successfully achieved even considering rapidly changing atmosphere. Through numerical simulations and real-time experiments, the better MPPT performance has been obtained compared with a traditional method. For a controller with lower response and unprecise control like PI controller, it reduces the generated power and provides only near-maximum power generation. Compared with the conventional PI control approach and open-loop system, the power extracted using TSMC is 10% and 209% higher, respectively. Therefore, the TSMC-based MPPT control method assures better tracking performance and high robustness.

Acknowledgment

This work was supported by the National Science Council, ROC, under Grants NSC-99-2221-E-033-055 and NSC-99-2632-E-033-001-MY3.

Appendix A. Proof of Theorem 1

Considering the Lyapunov function $V_s = \frac{1}{2}s^2$, the time derivative of V_s along the error dynamics (19) satisfies

$$\dot{V}_s = s\dot{s} = -Krse_2^{r-1}\text{sign}(s) = -Kre_2^{r-1}|s| \tag{29}$$

where $e_2^{r-1} = e_2^{\frac{p-q}{q}} > 0$ for all $e_2 \neq 0$. Under the situation $e_2 \neq 0$, $\dot{V}_s < -\delta|s|$ is satisfied for some $\delta > 0$. If considering $e_2 = 0$ and $s \neq 0$, the dynamics of e_2 submitted with the control law (18) is obtained below

$$\dot{e}_2 = -\frac{\alpha}{rC_1}e_2^{2-r} - K\text{sign}(s) = -K\text{sign}(s) \tag{30}$$

where $e_2 = 0$ is used. In other words, $\dot{e}_2 = -K$ for $s > 0$ and $\dot{e}_2 = K$ for $s < 0$. Furthermore, s does not change signs before the surface reaches zero ($s = 0$). The error e_2 moves away from zero in finite time once $s \neq 0$. Therefore, s satisfies $\dot{V}_s < -\delta|s|$ and tends to zero in finite time. This implies that e_1 and e_2 also converges to zero in finite time. As a result, the MPP voltage tracking is achieved with finite-time stabilizing. □

Appendix B. Proof of Theorem 2

To prove the stability of (26), consider the Lyapunov function $V_s = \frac{1}{2}s^2$ and taking the time derivative of V_s along (26). The following is obtained,

$$\begin{aligned}
\dot{V}_s &= sre_2^{r-1}\left(\Delta f - \Delta h_c - g_1\hat{g}_1^{-1}K^*\text{sign}(s)\right) \\
&\quad + sre_2^{r-1}(g_1 - \hat{g}_1)\hat{g}_1^{-1}\left(\frac{-\alpha e_2^{2-r}}{rC_1} - \hat{f}_1 + \hat{h}_c\right) \\
&\leqslant -\eta r|s||e_2^{r-1}| + r|s||e_2^{r-1}|(|\Delta f_1| + |\Delta h_c| + \eta) \\
&\quad - K^*r\varpi^{-1}|s||e_2^{r-1}| \\
&\quad + r|\varpi - 1||s||e_2^{r-1}|\left(\frac{\alpha}{rC_1}|e_2^{2-r}| + |\hat{f}_1| + |\hat{h}_c|\right)
\end{aligned}$$

If the control gain (27) is satisfied, then $\dot{V}_s \leqslant -\eta r|s||e_2^{r-1}|$. Therefore, as for the finite time convergence of the tracking errors, it is similar to the proof of Theorem 1. The terminal sliding mode control of the MPP voltage tracking is achieved with robustness. □

References

Altasa, I.H., Sharaf, A.M., 2008. A novel maximum power fuzzy logic controller for photovoltaic solar energy systems. Renewable Energy 33, 388–399.

Barambones, O., Etxebarria, V., 2002. Energy-based approach to sliding composite adaptive control for rigid robots with finite error convergence time. International Journal of Control 75 (5), 352–359.

Chang, E.C., Liang, T.J., Chen, J.-F., Chang, F.-J., 2008. Real-time implementation of grey fuzzy terminal sliding mode control for PWM DC–AC converters. IET Power Electronics 1 (2), 235–244.

Feng, Y., Yu, X.H., Man, Z., 2002. Non-singular terminal sliding mode control of rigid manipulators. Automatica 38, 2159–2167.

Hua, C.C., Lin, J.R., Shen, C.H., 1998. Implementation of a DSP-controlled photovoltaic system with peak power tracking. IEEE Transactions on Industrial Electronics 45 (1), 99–107.

Huang, X.Q., Lin, W., Yang, B., 2005. Global finite-time stabilization of a class of uncertain nonlinear systems. Automatica 41 (5), 881–888.

Hussein, K.H., Muta, I., Hoshino, T., Osakada, M., 1995. Maximum photovoltaic power tracking: an algorithm for rapidly changing atmospheric condition. IEE Proceedings – Generation Transmission and Distribution 142 (1), 59–64.

Kim, I.S., 2007. Robust maximum power point tracker using sliding mode controller for the three-phase grid-connected photovoltaic system. Solar Energy 81, 405–414.

Koutroulis, E., Kalaitzakis, K., Voulgaris, N.C., 2001. Development of a microcontroller-based, photovoltaic maximum power point tracking control system. IEEE Transactions on Power Electronics 16 (1), 46–54.

Kottas, T.L., Boutalis, Y.S., Karlisa, A.D., 2006. New maximum power point tracker for PV arrays using fuzzy controller in close cooperation with fuzzy cognitive networks. IEEE Transactions on Energy Conversion 21 (3), 793–803.

Krein, P.T., Bentsman, J., Bass, R., Lesieutre, M.B.L., 1992. On th use of averaging for the analysis of power electronic systems. IEEE Transactions on Power Electronics, 182–190.

Lalouni, S., Rekioua, D., Rekioua, T., Matagne, E., 2009. Fuzzy logic control of stand-alone photovoltaic system with battery storage. Journal of Power Sources 193, 899–907.

Man, Z., Yu, X.H., 1997. Terminal sliding mode control of MIMO linear systems. IEEE Transactions on Circuits and Systems I: Fundamental Theory and Applications 44 (11), 1065–1070.

Min, J., Xu, Z., 2009. Backstepping control for a class of uncertain systems based on non-singular terminal sliding mode. In: Int. Conf. on Industrial Mechatronics and Automation, pp. 169–172.

Nema, P., Nema, R.K., Rangnekar, S., 2009. A current and future state of art development of hybrid energy system using wind and PV-solar: a review. Renewable and Sustainable Energy Reviews 13 (8), 2096–2103.

Parra-Vega, V., Hirzinger, G., 2004. Chattering-free sliding mode control for a class of nonlinear mechanical systems. International Journal of Robust and Nonlinear Control 11 (12), 1161–1178.

Patcharaprakiti, N., Premrudeepreechacharnb, S., Sriuthaisiriwong, Y., 2005. Maximum power point tracking using adaptive fuzzy logic control for grid-connected photovoltaic system. Renewable Energy 30, 1771–1788.

Petreus, D., Patarau, T., Daraban, S., Moga, D., Morley, B., 2011. A novel maximum power point tracker based on analog and digital control loops. Solar Energy 85, 588–600.

Qi, Z., Wang, S., Liu, G.C., Tian, G., 2009. Integrated control of energy management for stand-alone PV system. In: Asia-Pacific Power and Energy Engineering Conference, pp. 27–31.

Salameh, Z., Taylor, D., 1990. Step-up maximum power point tracker for photovoltaic arrays. Solar Energy 44 (1), 57–61.

Salas, V., Olias, E., Barrado, A., Lazaro, A., 2009. Review of the maximum power point tracking algorithms for stand-alone photovoltaic systems. Solar Energy Materials & Solar Cells 90, 1555–1578.

Slotine, J.-J.E., Li, W., 1991. Applied Nonlinear Control. Prentice-Hall, Englewood Cliffs, New Jersey.

Solodovnik, E.V., Liu, S., Dougal, R.A., 2004. Power controller design for maximum power tracking in solar installations. IEEE Transactions on Power Electronics 19 (5), 1295–1304.

Sun, J., Gratstollen, H., 1992. Averaged modeling of switching power converters: reformulation and theoretical basis. Power Electronics Specialists Conference, 1165–1172.

Taherbaneh, M., Faez, K., 2007. Maximum power point estimation for photovoltaic systems using neural networks. In: Proc. IEEE Int. Conf. Control Autom., pp. 1614–1619.

Tao, C.W., Taur, J.S., Chan, M.L., 2004. Adaptive fuzzy terminal sliding mode controller for linear systems with mismatched time-varying uncertainties. IEEE Transactions on Systems, Man, and Cybernetics, Part B: Cybernetics 34 (1), 255–262.

Veerachary, M., Senjyu, T., Uezato, K., 2003. Neural-network-based maximum-power-point tracking of coupled-inductor interleaved-boost-converter-supplied PV system using fuzzy controller. IEEE Transactions on Industrial Electronics 50 (4), 749–758.

Venkataraman, S.T., Gulati, S., 1993. Control of nonlinear systems using terminal sliding modes. ASME Journal of Dynamic Systems, Measurement and Control 115, 554–560.